water

MDPI

Article

Dynamics of Water Vapor Content around Isolated Sprinklers: Description and Validation of Model

Jian Jiao, Derong Su * and Yadong Wang

Research Center for Grassland Ecology and Resources, Beijing Forestry University, No. 35 Tsinghua East Road, Beijing 100083, China; jiaojian@bjfu.edu.cn (J.J.); donglaswang@bjfu.edu.cn (Y.W.)

* Correspondence: suderong@bjfu.edu.cn; Tel.: +86-10-6233-6284

Academic Editor: Ashok K. Chapagain

Received: 8 February 2017; Accepted: 24 April 2017; Published: 27 April 2017

Abstract: Irrigation consumes considerable water to satisfy the current food demand. An improvement in water use efficiency for irrigation is essential. Wind drift and evaporation losses reduce the water use efficiency of center pivot irrigation systems in arid and semi-arid areas. In this paper, a model of water vapor dynamics during and after overhead sprinkler irrigation was developed and validated by experimental data using a center pivot simulator and a water vapor measuring system. The model was represented as an exponential equation during irrigation and a logistic equation after irrigation. The water vapor dynamics measured next to and 2 m from the sprinkler were well-fitted with the developed model. Model performance was good according to evaluations of the Nash—Sutcliffe efficiency coefficient, with values of 0.961 and 0.934 for estimations next to the sprinkler and 2 m from the sprinkler, respectively. Results showed that both modeled and observed water vapor dynamics increased rapidly as irrigation started, and then leveled off to maximum values. After irrigation, the water vapor dynamics started to decrease gradually, and eventually decreased rapidly. The decreasing rate stopped when the water vapor content was restored to the level of the surrounding atmosphere. The model parameters showed that the maximum increases in water vapor content were from 2.506 to 6.476 g m^{-3} for the area next to the sprinkler, and 1.277 to 3.380 g m^{-3} for the area 2 m from the sprinkler, under the influence of vapor pressure deficits. The increasing and decreasing rates of the dynamics during and after irrigation were influenced by temperature, relative humidity, and vapor pressure deficits, according to Pearson's correlations. A period of 2.3 to 4.0 h was required to restore water vapor to the atmospheric level.

Keywords: sprinkler irrigation; wind vapor dynamics; dynamic model; evaporation losses

1. Introduction

Irrigation plays a crucial role in supplying sufficient water to increase crop yield and quality, which is a major driver of water consumption and change [1,2]. Irrigation is the human activity that consumes most water nowadays [3,4]; it could even lead to intensified hydrological drought [5], which might be a severe issue for arid areas. The area of irrigated alfalfa (*Medicago sativa* L.) in China has increased rapidly since 2012 and has reached over 4 million hectares [6]. This area is mainly distributed in the northwestern and northern regions of the country, which are characterized by arid and semiarid climates [7]. In order to reduce water consumption and increase application efficiency, center pivot sprinkler irrigation (center pivot) is the most popular system [8,9] in the production of alfalfa in the arid and semiarid areas.

On center pivots, sprinklers are hung below the lateral pipes [10], which are used as a water supply. Center pivots represent a typical pattern of overhead sprinkler irrigation [11,12]. During the operation of a single sprinkler, a stream of water is deflected by a spray plate, to disperse water into multiple streams [13]. Multiple water streams are then sprayed from the sprinkler at a high velocity

into the surrounding air, and friction between the air and the water streams causes the water streams to break apart into water droplets [14]. Most of the water droplets will reach the plant canopy or soil surface, whereas a fraction of the droplets will evaporate and turn into water vapor before reaching the plant canopy or soil surface [15,16]. The evaporated water vapor is regarded as wind drift and evaporation losses (WDELs) [17]. Under drought climates, WDELs are among of the important factors contributing to a reduction in irrigation water-use efficiency [15,18].

WDEL measurement commonly use a catch can test, which is a standard international test [19,20], based on the water balance principle. That is, a series of catch cans is arranged at the canopy height, and the variation in water volume between catch cans and sprinkler irrigation volumes is designated as WDELs [16,21–25]. By this means, researchers have reported different levels of WDELs during crop canopy sprinkler irrigation. Values of WDELs reaching 10.9% and 3.7% of applied water during daytime and nighttime, respectively, have been reported in alfalfa canopies [16], and 8.2–13.6% and 3.3–8.0% of irrigation volumes during the daytime and nighttime, respectively, have been reported for beet (*Beta vulgaris* L.) canopies when using a commercial center pivot [24]. Observations conducted in a maize (*Zea mays* L.) canopy yielded WDEL values of 19.3% and 8.1% during the daytime and nighttime, respectively [26].

However, dozens to hundreds of catch cans are generally required to complete WDEL measurements [16,27,28]. In addition, the water volumes collected by each catch can must be measured immediately, as irrigation completes, to limit evaporation of collected water [21,23]. Catch can measurement therefore requires a massive labor force and is inefficient [29]. For this reason, alternative observation methods have been advocated, e.g., the electrical conductivity method [30], chemical tracer methods using potassium ion [31] and eddy covariance measurements [32].

A convenient and easy way to estimate water-use efficiency is to build mathematical models to estimate WDELs. Many studies have shown that meteorological conditions have a significant influence on WDELs. Thus, many empirical models have been developed to estimate WDELs by using wind speed as a single variable [22–24,28,33–35], and several models have included wind speed and other meteorological variables, such as temperature [13,23,27], relative humidity [23] and vapor pressure deficit [21,36] as parameters. Theoretical models have also been built to incorporate droplet ballistics dynamics and evaporation [37,38]. These models have mainly focused on estimating evaporation losses and water-use efficiency for an irrigation event. However, over the irrigation period, Those models are unavailable to present the developing processes of WDEL, which may be expressed as the water vapor dynamics around the sprinkler. Few studies have paid particular attention to the water vapor dynamics, because catch can tests provide only a single data point following the experiments [29], making it impossible to capture the continuous variation in water vapor content. However, water vapor dynamics are closely related to the generating processes of WDELs; accurate representation of such development features will help to effectively decrease WDELs.

Temporal variation of water vapor content during irrigation has been briefly mentioned in previous studies, but its spatial variation within irrigated area has not been focused on specifically. Playán et al. [23] reported an obvious increase in absolute humidity (AH) during irrigation using a solid sprinkler, and relative humidity increased by 3.9% and temperature decreased by 0.5 °C within the irrigated area. Liu and Kang [39] observed a temperature decrease of 1.8–3.9 °C in a winter wheat (*Triticum aestivum* L.) canopy with sprinkler irrigation. Wang et al. [40] studied winter wheat and summer maize canopies and found a rapid increase in relative humidity, ranging from 3–13%, after initiating irrigation. These studies reported differences in water vapor content and temperature, when comparing the irrigated area to the surrounding area. However, details of the temporal dynamics and spatial variations of the water vapor content during a sprinkler irrigation event are lacking, even in descriptive models. Conversely, Sadeghi et al. [29] provided new methodology called a 'strip test' to monitor the dynamic variation in WDELs under a center pivot irrigation system. However, the published results did not provide a theoretical model of the dynamic variation.

Thus, it should be meaningful to explore the water vapor dynamics during sprinkler irrigation, which are relevant to the generating processes of WDEL. This work should be helpful to determine the occurrence mechanism of WDEL, so as to find effective ways to reduce WDEL. The objectives of this study were to (i) develop a model to describe the water vapor dynamics for single sprinkler irrigation; the model could be available to describe water vapor dynamics at different distances from the sprinkler and at any time during and after irrigation; (ii) to validate the dynamic model through experimental observations, using a center pivot simulator and a water vapor measuring system.

2. Theoretical Considerations

2.1. Vapor Pressure Deficit

Evaporation occurs from the streams sprayed from a sprinkler, until it reaches the crop or soil surface [23,26]. This process increases the water vapor content within the irrigation area. Water vapor content was represented as value of absolute humidity (AH; g m^{-3}) in the following equation [41]:

$$AH = \frac{P_W}{R_W \cdot T_K} \cdot 10^6 \quad (1)$$

where P_W is actual vapor pressure (kPa), R_W is a gas constant of water (461.52 J kg^{-1} K^{-1}) [41], and T_K is the Kelvin temperature (K).

In addition, the saturation vapor pressure, P_{WS} (kPa) is calculated according to the following equation [42]:

$$P_{WS} = 0.6108 \exp\left(\frac{17.27T}{T + 17.27}\right) \quad (2)$$

where T is temperature (°C).

The difference between P_{WS} and P_W is the vapor pressure deficit (VPD; kPa) given by

$$VPD = P_{WS} - P_W \quad (3)$$

2.2. Water Vapor Dynamics during Irrigation

When irrigation is initiated, the VPD is relatively high and the increasing rate of water vapor accumulation is rapid during this period. With continuous irrigation, the VPD should gradually decrease and the increasing rate of water vapor content gradually decreases, to the saturated state. The water vapor continues to drift and diffuse from the irrigated area in an open space. The water vapor increment generated by irrigation (the different water vapor content between irrigated area and surrounding atmosphere) were used to describe water vapor variations and dynamics. Assuming stable temperature, relative humidity and calm wind, water vapor increment could reach a stable state and a maximum level, until the increasing rate of water vapor accumulation equals the rate of water vapor drift. Thus, with the assumption that A is the water vapor increment at any time, and A_{m1} is the maximum value of A, a differential equation has been derived to indicate that, at any given time, the increasing rate of water vapor increment is proportional to the difference between the maximum water vapor increment, A_{m1} (g m^{-3}), and the current water vapor increment, A (g m^{-3}), given by

$$\frac{dA}{dt} = k(A_{m1} - A) \ (t \geq 0) \quad (4)$$

where t is the irrigation time duration (h), dA/dt is the increasing rate of change of water vapor increment (g m^{-3} h^{-1}), and k is the exponential coefficient of water vapor increment (h^{-1}).

When t = 0, the water vapor contents inside and outside the irrigated area are equal, namely A = 0 (water vapor increment is zero). Thus, the solution of differential Equation (4) results in:

$$A(t) = A_{m1}(1 - e^{-kt}) \ (0 \leq A \leq A_{m1}, \ t \geq 0) \quad (5)$$

Equation (5) is the dynamic model of water vapor increment during sprinkler irrigation, in which the parameters, A_{m1} and k, can be determined through experiments.

2.3. Water Vapor Dynamics after Irrigation

After the completion of irrigation, no additional water vapor will be generated within the irrigated area. With the drift of water vapor, the content of water vapor within the irrigated area will be reduced, and it will gradually be restored to the level of the surrounding atmosphere. This means that the water vapor increment should become lower and lower, approaching zero, after irrigation. This procedure could be explained by the principle of the logistic function [43,44]. According to the logistic function, if the decreasing rate is expressed as a function $f(A)$, in terms of A, then

$$\frac{dA}{dt'} = -f(A) \cdot A \tag{6}$$

where A is water vapor increment at any time (g m^{-3}), t' is decreasing time duration of A (h), or the duration after irrigation, dA/dt' is the rate of decrease in water vapor increment (g m^{-3} h^{-1}), $f(A)$ is the function in terms of A, and the minus sign indicates the decreasing trend of A. It should be noted that $t' = 0$ corresponds to the time when irrigation is completed (defined as t_s) or when A begins to decline.

The $f(A)$ can be expressed as a line function, with respect to A:

$$f(A) = r - s \cdot A \ (r > 0,\ s > 0) \tag{7}$$

where r is the intrinsic rate of decrease [45] of A (h^{-1}) and s is a parameter of the function.

Additionally, A_{m2} can be referred to as the carrying capacity [44] of water vapor increment, and it is the theoretical maximum value for the logistic function. A_s is defined as the value of A when irrigation is completed or the initial value when A begins to be reduced just after irrigation. Thus, when $t' = 0$ (the time point when irrigation is completed and A begins to reduce), then $A = A_s$ and $A_s < A_{m2}$. When $A = A_{m2}$, the decreasing rate of A should equal 0, and, as a result, $f(A_{m2}) = 0$. To substitute for Equation (7):

$$s = \frac{r}{A_{m2}} \tag{8}$$

Substitute Equation (8) into Equation (7):

$$f(A) = r\left(1 - \frac{A}{A_{m2}}\right) \tag{9}$$

To continue to substitute Equation (9) into Equation (6):

$$\frac{dA}{dt'} = -rA\left(1 - \frac{A}{A_{m2}}\right) \tag{10}$$

Equation (10) expresses the reduced regulation of water vapor increment after irrigation. Note that when $t' = 0$, then $A = A_s$. Thus, the solution of differential Equation (10) results in the following:

$$A(t\prime) = \frac{A_{m2}}{1 + \left(\frac{A_{m2}}{A_s} - 1\right) \cdot e^{rt\prime}} (t\prime \geq 0) \tag{11a}$$

Regulation should be a continuous process, according to the increasing and decreasing dynamics of water vapor increment during and after sprinkler irrigation; thus, when defining time t_s as the time required for the irrigating operation, Equation (11a) can be expressed as follows:

$$A(t) = \frac{A_{m2}}{1 + \left(\frac{A_{m2}}{A_s} - 1\right) \cdot e^{r(t - t_s)}} \ (t \geq t^s) \tag{11b}$$

Equation (11b) is the dynamic model of water vapor increment after sprinkler irrigation, in which parameter t_s represents the length of time of irrigation. The parameters A_{m2}, A_s, and r can be estimated from experimental data.

Equations (5) and (11b) should be a continuous function in the interval of $t > 0$. Therefore, the value of A_s should explain why Equation (5) is equal to Equation (11b), where $t = t_s$:

$$A_s = A_{m1}(1 - e^{-kt_s}) \tag{12}$$

2.4. Overall Water Vapor Dynamics

By combining Equations (5) and (11b), a complete model for the dynamics of water vapor increment during and after sprinkler irrigation is described as follows:

$$A(t) = \begin{cases} A_{m1}(1 - e^{-kt}) \ (0 < t \leq t_s) \\ \frac{A_{m2}}{1 + \left(\frac{A_{m2}}{A_s} - 1\right) \cdot e^{r(t - t_s)}} (t \leq t) \end{cases} \tag{13}$$

The dynamics of water vapor increment during and after sprinkler irrigation are shown in Figure 1, according to the model (Equation (13)). It can be seen that the increasing rate of water vapor increment, caused by irrigation, is extremely high at the initiation of irrigation, and then gradually decreases toward the value of A_s, reaching a relatively stable level. After the completion of irrigation, the value of A starts to decrease gradually at first; then the deceasing trend continues, and finally gradually stabilizes at zero, which means that water vapor contents of the inner and outer irrigated areas gradually become consistent.

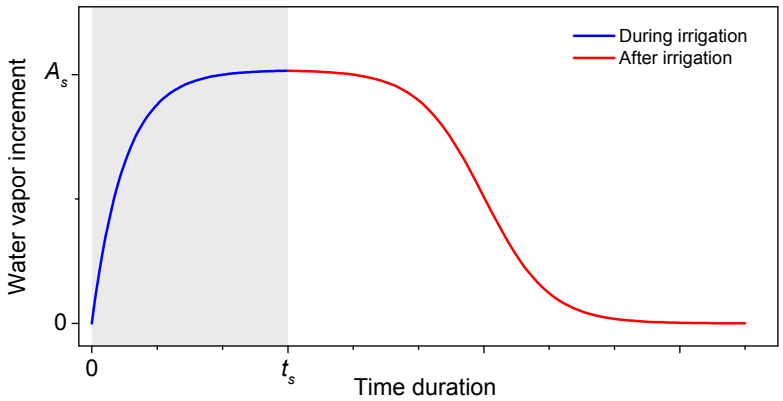

Figure 1. Dynamics of water vapor increment during (blue line) and after (red line) irrigation. The shaded area indicates the irrigation periods. A_s is water vapor increment when irrigation is finished, and t_s is the length of time of the irrigation operation.

3. Materials and Methods

3.1. Experimental Site

This experiment was conducted at the Shuangqiao Experimental Station, Clover Grass Industry Technology Development Center, located in the Tongzhou District of Beijing, China (116°61′ N latitude

and 39°88′ E longitude, and 50 m a.s.l.). The experimental station covered an area of 18 ha, encircled by windbreaks. The irrigated field was a 20 m × 20 m flat block, being located at the center of the station. Alfalfa (*Medicago sativa* L.) was planted in the irrigated field; seeds were sown on 9 April 2015. During the experimental season, the alfalfa was regularly irrigated as agronomical practices were performed (fertilization, weeding, application of insecticides, and harvest cutting).

The experiments were carried out during low-wind days, from August to November 2015. All irrigation events were carried out during the period of lowest relative humidity and highest temperature during the daytime [26,46], corresponding to the daily maximum evaporative demand. Sprinkler irrigation was started at 1:30 p.m. and finished at 2:30 p.m. local time, a duration of 1 h.

3.2. Simulator for Single Sprinkler

A supporting frame was set up to functionally simulate a center pivot sprinkler irrigation system (Figure 2). The supporting frame was 800 cm long and 230 cm high. A test sprinkler was placed below the center of the beam of the supporting frame, at a height of 100 cm above the ground. A pump (model QD6-35/2-1.5J; Shimge Pump Industry Co., Taizhou, China) with maximum pressure of 343.2 kPa and flow rate of 6 m^3 h^{-1} was used to supply water. Pressure gauges (model YB-150B; ZOHA Co., Xi'an, China) and valves (Φ25 mm ball valve; Huaya Co., Ningjin, China) were installed along pipes to control water pressure. A mesh filter (Modular 100; AZUD Co., Murcia, Spain) was installed to prevent the nozzle from clogging. A pressure regulator (15 PSI; Nelson irrigation Co., Walla Walla, WA, USA) was installed upstream of the test sprinkler to maintain a stable pressure of 105 kPa.

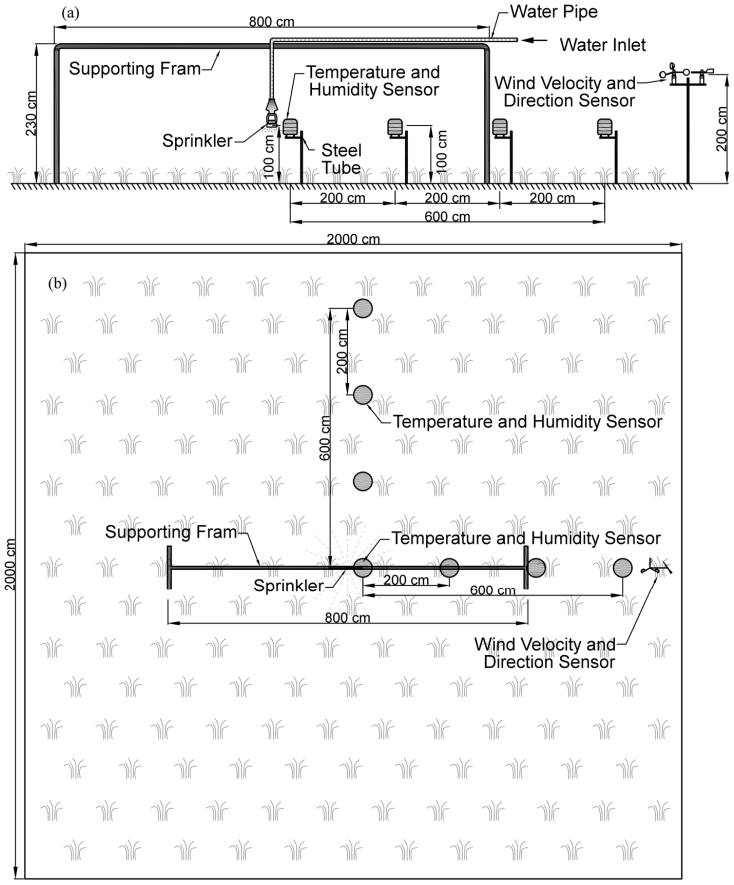

Figure 2. Diagram of the sprinkler simulator for the center pivot irrigation system and water vapor measuring system: (**a**) side view and (**b**) top view. The irrigated field was plated with alfalfa (*Medicago sativa* L.).

The sprinkler was a fixed spray plate sprinkler (model: D3000; Nelson irrigation Co., Walla Walla, WA, USA). The nozzle diameter was 4.76 mm, and a blue spray plate was installed. The concave sprinkler plate deflected 36 streams to form a uniform circular spray, with a slight angle. The wetted radius was approximately 4.9 m, when the sprinkler height was 100 cm.

3.3. Water Vapor Measuring System

A water vapor measurement system was designed and built by the authors for the experiment. It consisted of three main parts (Figure 3): (1) eight digital temperature and relative humidity sensors (model SHT75; Sensirion AG, Staefa, Switzerland), with accuracies of ±0.3 °C (10 °C–40 °C) for temperature, ±1.8% for relative humidity from 10% to 90%, and ±1.8% to ±4.0% for relative humidity from 90% to 100%; (2) a pair of wind speed and wind direction sensors (models YGC-FS and YGC-FX, respectively; Yigood Technology, Wuhan, China), with accuracies of 0.3 m/s and ±1%, respectively; and (3) a data logger, which we built using a single-chip microcomputer, digital clock and digital logger. All the temperature and relative humidity sensors (sensors) and wind speed and wind direction sensors were connected to the data logger by signal cables; RS-485 Bus was used to connect the sensors and the data logger.

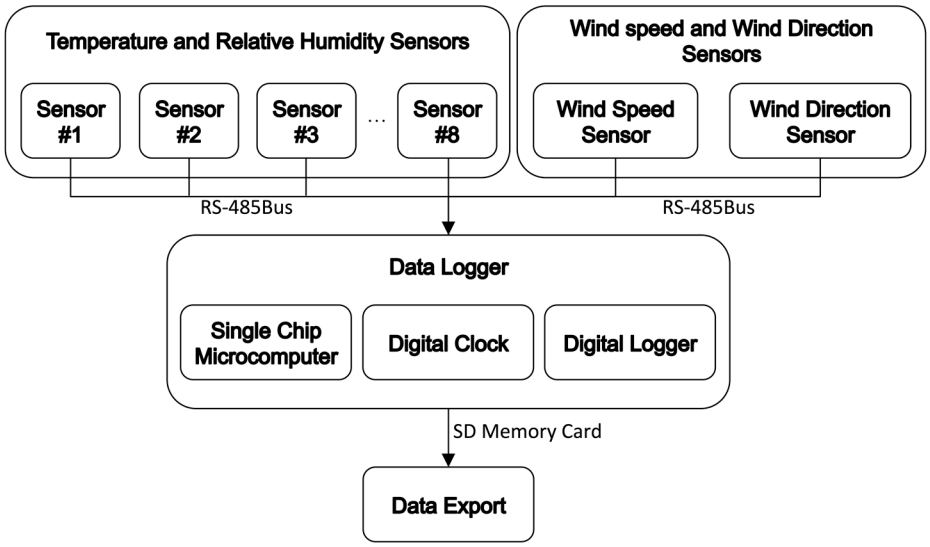

Figure 3. Schematic diagram of our water vapor measurement system.

Seven of the sensors were arranged within the irrigated field. As shown in Figure 2, the first sensor was placed next to the sprinkler, and then additional sensors were placed at intervals of 2 m along two perpendicular radii of a circle, centered at the test sprinkler. Each sensor was fixed to a steel pipe, inserted firmly into the soil. All sensors were positioned at a height of 100 cm, the same height as the test sprinkler. The remaining sensor was installed 50 m away from the irrigated field to measure the relative humidity and temperature of the surrounding atmosphere (not shown in Figure 2), which were referenced as meteorological parameters. Wind speed and direction sensors were installed within the irrigated area and mounted 2 m above the ground. All of the sensors probes were wrapped with a special material, which provided water insulation and air permeability so that the sensors could operate properly during irrigation.

The data logger recorded 5 min average values of temperature, relative humidity, wind speed, and wind direction, based on five single readings (once per minute) over a 5 min period. Two data series recorded from the paired sensors, which were at two perpendicular radii as well as equal distance from the sprinkler, were averaged to form one single data series to represent water vapor dynamics at that distance.

3.4. Statistics Processing and Analysis

The amounts of water vapor increment were quantified by the value of absolute humidity (*AH*; g m^{-3}). The *AH* was calculated based on the temperature and relative humidity data collected by the sensors. The relative humidity is defined as the ratio of actual to saturation water vapor pressure at gas temperature:

$$RH = \frac{P_W}{P_{WS}} \cdot 100\% \tag{14}$$

Therefore, Equation (1) also could also be expressed as follows:

$$AH = \frac{RH \cdot P_{WS}}{R_W \cdot T_K} \cdot 10^6 \tag{15}$$

The value of P_{WS} calculated from the temperature (T) data as in Equation (2) was substituted into Equation (15), to compute *AH*. Then, the *AH* of position next to sprinkler, and 2 m, 4 m and 6 m away from sprinkler, can be calculated according to data of *RH* and *T* measured by corresponding sensors. The *AH* of surrounding atmosphere can also be calculated according to data of *RH* and *T* measured by the sensor located 50 m away from the irrigated field. Then, the water vapor increment caused by irrigation (A) can be calculated as follows:

$$A_d = AH_d - AH_{sa} \tag{16}$$

where d indicates the distance away from sprinkler, A_d represents water vapor increment at d m from sprinkler (g m^{-3}), AH_d is absolute humidity at d m from sprinkler (g m^{-3}), and AH_{sa} is absolute humidity of surrounding atmosphere (g m^{-3}).

The VPD (kPa) was used as a meteorological parameter, together with temperature and relative humidity. It can be calculated by combining Equations (2), (3), and (14), using the relative humidity and temperature data collected by the sensor located 50 m away from the irrigated field.

Nonlinear regression was used to fit the model and experimental results (during and after sprinkler irrigation), to estimate the model parameters A_{m1}, k, A_{m2}, A_s, and r. The fitting significance between developed model and experimental data was judged according to the f-test. The relationships between model parameters and meteorological factors were analyzed by computing Pearson's correlation coefficients. Model performance was evaluated quantitatively using the Nash–Sutcliffe model efficiency (NSE) coefficient [47], calculated as follows:

$$\mathrm{NSE} = 1 - \frac{\sum_{i=1}^{n} (A_{o,i} - A_{e,i})^2}{\sum_{i=1}^{n} \left(A_{o,i} - \overline{A_o}\right)^2} \tag{17}$$

where n is the total number of time steps, $A_{o,i}$ is the observed value at time step i, $A_{e,i}$ is the estimated value at time step i based on the model, and $\overline{A}_o$ is the mean of observed values. Evaluation criteria for the levels of model performance were in accordance with Ritter and Muñoz-Carpena [48]; the equations were as follows:

$$n_t = \frac{SD}{RMSE} - 1 \tag{18}$$

$$\mathrm{NSE} = 1 - \left(\frac{1}{n_t + 1}\right)^2 \tag{19}$$

where the *RMSE* is the root mean square error, *SD* is the standard deviation of observations, and the n_t is the number of times that the observation variability was greater than the mean error. *RMSE* and *SD* are given, respectively, by

$$RMSE = \sqrt{\frac{1}{n}\sum_{i=1}^{n}(A_{o,i} - A_{e,i})^2} \quad (20)$$

and

$$SD = \sqrt{\frac{1}{n}\sum_{i=1}^{n}\left(A_{o,i} - \overline{A_o}\right)^2} \quad (21)$$

If the value of n_t is higher than 2.2 and the value of NSE is higher than 0.90, then it can be stated that the model performance is very good [48]. Statistical analyses were performed using OriginPro (ver. 9.2; OriginLab Corp., Northampton, MA, USA) [49].

3.5. General Characteristics of the Experiments

A total of seven tests were performed due to low wind conditions (<0.9 m/s). The detailed meteorological parameters of these tests are listed in Table 1. Because temperatures were dropping, the results in general show decreasing relative humidity, temperature, and VPD.

Table 1. Meteorological parameters of seven available tests.

Tests	Date	RH (%)	T (°C)	W (m s^{-1})	VPD (kPa)
1	29 August	44.18	31.09	0.70	2.521
2	3 September	43.10	31.80	0.81	2.675
3	21 September	42.59	28.05	0.52	2.176
4	3 October	41.75	24.58	0.89	1.800
5	9 October	20.81	19.70	0.90	1.818
6	14 October	48.21	21.75	0.80	1.349
7	1 November	31.07	17.29	0.84	1.360

Notes: RH, relative humidity; T, temperature; W, wind speed; VPD, vapor pressure deficit. The RH, T was measured by the sensor located 50 m away from irrigated area, the W was measured by the wind speed sensor located within irrigated area (Figure 2) and the VPD was calculated based on the RH and T.

4. Results and Discussion

4.1. Water Vapor Dynamics

Figure 4 shows the water vapor dynamics of tests on 3 September, 3 October and 14 October, which represented relatively high, medium and low levels of VPD (2.675, 1.800 and 1.349 kPa respectively) for irrigated fields [50–52]. In addition, the values of water vapor increment, measured by sensors located 4 and 6 m from the sprinkler, were low and could not be fit properly with the model. Therefore, the fitting results for these two measuring sites are not shown in Figure 4 and Table 2. The fitting results suggested that the sprinkler influenced the water vapor content within 4 m, which is less than its water application distance [13,53].

In general, during irrigation, the water vapor increment initially increased rapidly, and then reached a relative stable state until completion of irrigation. At the conclusion of irrigation, the water vapor increment reduced gradually at first and then started to decline rapidly. The rate of reduction of water vapor increment decreased and gradually reduced to zero, as the water vapor content in the irrigated field was restored to the level of the surrounding atmosphere.

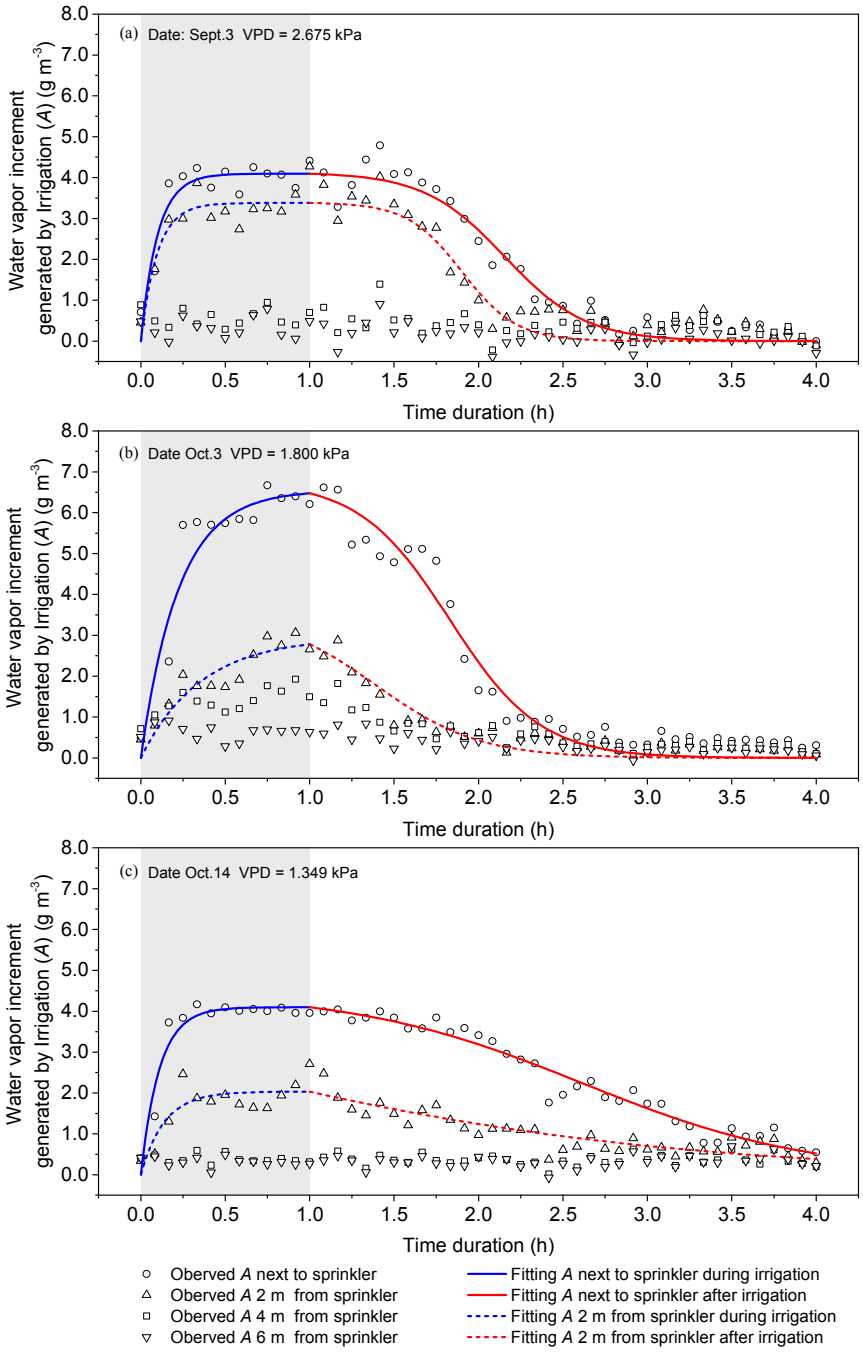

Figure 4. Observed values and fitting results based on the water vapor dynamics model during irrigation (blue lines) and after irrigation (red lines). A is the water vapor increment generated by irrigation. The shaded area indicates the 1 h irrigation periods.

Water vapor dynamics differed between areas next to and 2 m from the sprinkler. During irrigation, both the increasing rate and amount of water vapor increment were higher for areas next to the sprinkler than areas 2 m from the sprinkler. These results were reflected in higher values of k and A_{m1}, respectively, among the model parameters. After irrigation, the water vapor increment 2 m from the sprinkler generally changed faster than those next to the sprinkler. This may be because the value of water vapor increment next to the sprinkler was relatively higher than that 2 m from the sprinkler, such that the higher water vapor content would be more likely to diffuse to the surroundings [54] once water vapor stopped being generated (after irrigation).

Table 2. Coefficients and fitting parameters of the model.

Date	Distance (m)	Model: During Irrigation $A(t) = A_{m1}(1 - e^{-kt})$ $0 < t \leq t_s$				Model: After Irrigation $A(t) = \frac{A_{m2}}{1+\left(\frac{A_{m2}}{A_s}-1\right)\cdot e^{r(t-t_s)}}$ $t \geq t_s$					
		A_{m1} (g m^{-3})	k (h^{-1})	$R_a{}^2$	p	A_{m2} (g m^{-3})	A_s (g m^{-3})	r (h^{-1})	t_s (h)	$R_a{}^2$	p
29 August	0	2.746	17.675	0.894	<0.001	2.769	2.746	4.015	1	0.960	<0.001
	2	2.808	7.599	0.944	<0.001	3.430	2.806	2.593	1	0.971	<0.001
3 September	0	4.096	10.103	0.858	<0.001	4.129	4.096	4.174	1	0.956	<0.001
	2	3.380	10.320	0.790	<0.001	3.393	3.380	6.176	1	0.901	<0.001
21 September	0	2.682	7.957	0.673	<0.001	2.921	2.681	1.902	1	0.974	<0.001
	2	2.609	5.300	0.756	<0.001	4.868	2.596	1.765	1	0.935	<0.001
3 October	0	6.552	4.449	0.898	<0.001	6.769	6.476	3.731	1	0.966	<0.001
	2	2.958	2.822	0.808	<0.001	3.545	2.782	3.271	1	0.912	<0.001
9 October	0	5.842	3.403	0.868	<0.001	5.768	5.648	6.460	1	0.980	<0.001
	2	3.426	3.394	0.817	<0.001	3.672	3.311	4.206	1	0.952	<0.001
14 October	0	4.094	9.010	0.925	<0.001	4.474	4.094	1.471	1	0.966	<0.001
	2	2.029	7.209	0.644	<0.001	6.106	2.028	0.672	1	0.759	<0.001
1 November	0	2.557	3.930	0.862	<0.001	2.778	2.506	1.883	1	0.969	<0.001
	2	1.322	3.370	0.947	<0.001	1.357	1.277	2.334	1	0.957	<0.001

Notes: The second column means radial distance from sprinkler: 0 and 2 m indicate distance away from the test sprinkler. A, water vapor increment generated by irrigation at any time (g m^{-3}); t, time from the start of irrigation (h); A_{m1}, maximum value of water vapor increment during irrigation (g m^{-3}); k, exponential coefficient of water vapor increment during irrigation (h^{-1}); $R_a{}^2$, adjusted coefficients of determination; P, fitting significance, according to the f-test; A_{m2}, carrying capacity of the logistic equation, theoretical maximum value of water vapor increment after irrigation (g m^{-3}); A_s, value of water vapor increment at the conclusion of irrigation (g m^{-3}); r, exponential coefficient of water vapor increment after irrigation (h^{-1}); t_s, time length of irrigation operation (h).

4.2. Water Vapor Dynamics and Meterorology

The height of the curves reflected the amount of water vapor increment. The higher the values of VPD, the greater the water vapor increment for 2 m from the sprinkler. The value of A_{m1} (2 m from the sprinkler) declined with reduced VPD, with a Pearson's correlation coefficient of 0.68 ($p < 0.05$; Figure 5b). Similarly, at the conclusion of irrigation, the value of A_s (2 m from the sprinkler) was reduced with declining VPD, with a Pearson's correlation coefficient of 0.73 ($p < 0.05$; Figure 5b). However, there was no significant relationship between A_{m1} (next to the sprinkler) and VPD, or between A_s (next to the sprinkler) and VPD.

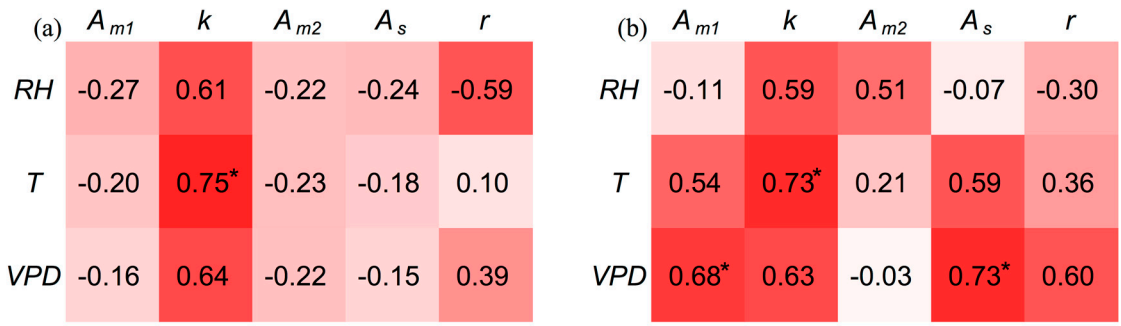

Figure 5. Pearson's correlation between meteorological conditions and model parameters: (**a**) next to the sprinkler, and (**b**) 2 m from the sprinkler. *RH*, *T*, and *VPD* indicate the relative humidity, temperature, and vapor pressure deficits, respectively. The A_{m1}, k, A_{m2}, A_s and r are model parameters. The color depth of redness indicates the extent of correlation, according to the correlation coefficient values, and the asterisks indicate significance ($p < 0.05$).

The reasons why VPD had less influence on A_{m1} and A_s next to the sprinkler are possibly due to intensive water spray and mist diffusion next to the sprinkler, and weak restriction of water vapor content under the meteorological conditions. Nevertheless, the air 2 m from the sprinkler was more influenced by meteorological conditions. As a result, the surrounding meteorological factors had a major influence on the area 2 m from the sprinkler. In this experiment, the VPD and water vapor increment (A_{m1} and A_s; 2 m from the sprinkler) were positively and significantly correlated, consistent with previous reports on the relationship between evaporation losses and the VPD [16,21,23,55,56].

The values of k reflected increasing rates of change in water vapor increment during irrigation. The value of k (next to the sprinkler) increased significantly with increasing temperature, with a Pearson's correlation coefficient of 0.75 ($p < 0.05$; Figure 5a). The VPD positively influenced the value of k (next to the sprinkler), at least to some extent (Figure 5a). A similar trend was observed for observations 2 m from the sprinkler (Figure 5b).

The decreasing rates of water vapor increment after irrigation could be reflected in the value of r. The value of r (next to the sprinkler) tended to increase with decreasing relative humidity and increasing VPD (Figure 5a). The value of r (2 m from the sprinkler) tended to increase with increasing VPD (Figure 5b). Therefore, relative humidity and VPD could affect the time required for water vapor to be restored to the level of the surrounding atmosphere following irrigation. For all of the tests, restoration required approximately 2.3 to 4.0 h (Figure 4); this duration was similar to that for observations based on maize [52,57,58] and alfalfa [16].

4.3. Water Vapor Increment

The model parameters A_{m1}, A_{m2} and A_s (Table 2) reflected the water vapor increment generated by irrigation. The values of A_{m1} and A_{m2} would probably be unequal, due to experimental errors and measurement fluctuations. Next to the sprinkler, A_{m1} ranged from 2.557 to 6.552 g m^{-3}, A_{m2} ranged from 2.769 to 6.769 g m^{-3}, and A_s ranged from 2.506 to 6.476 g m^{-3}, with no obvious differences between them. At 2 m from the sprinkler, the value of A_{m1} ranged from 1.322 to 3.426 g m^{-3}, A_{m2} ranged from 1.357 to 6.106 g m^{-3}, and A_s ranged from 1.277 to 3.380 g m^{-3}. The value of A_{m2} was slightly higher than that of A_{m1} and the value of A_{m1} was slightly higher than that of A_s. Generally, the water vapor increment were higher next to the sprinkler than 2 m from the sprinkler. With the value of A_s as a reference, the maximum amounts of water vapor increment were 2.506 to 6.476 g m^{-3} and 1.277 to 3.380 g m^{-3} next to and 2 m from the sprinkler, respectively.

In a previous study, Playan et al. [23] determined that irrigation could affect the meteorological variables within the irrigated plot, and they reported an increase of AH that ranged from approximately 2–3 g m^{-3} with solid sprinkler irrigation during the daytime, which was consistent with our value of A_s 2 m from the sprinkler, but lower than the value of A_s next to the sprinkler. This discrepancy may be due to the shorter distance between the observation site (A_s next to the sprinkler) and the sprinkler for sensors in the current experiment, compared with those at the meteorological station in the previous experiment [23].

4.4. Model Validation

The adjusted coefficient of determination (R_a^2) ranged from 0.644 to 0.947 and 0.759 to 0.980 (Table 2), during and after irrigation, respectively, at a significance level of $p < 0.001$. Therefore, the developed model was a good fit with actual observations and properly reflected the actual dynamics of water vapor increment. Under actual conditions, the meteorological conditions fluctuated and the water vapor of surrounding air was not uniform or stable [59], due to the interference of wind flow [60].

The comparisons between measured and calculated water vapor increment due to irrigation, for all of the available tests, are shown in Figure 6. The values of the Nash-Sutcliffe efficiency coefficient for the model were 0.961 and 0.934 for the estimations next to the sprinkler and for 2 m from the sprinkler, respectively (Table 3). These values suggested that the estimation was ideal and that model

performance was very good [48]; model performance was better for the estimation next to the sprinkler (Figure 6a) than for 2 m from the sprinkler (Figure 6b). The model performance was better than or in accordance with previous studies focusing on models of hydrology [61,62], crop coefficient [63], rainfall interception by canopy [64], and water use efficiency [65].

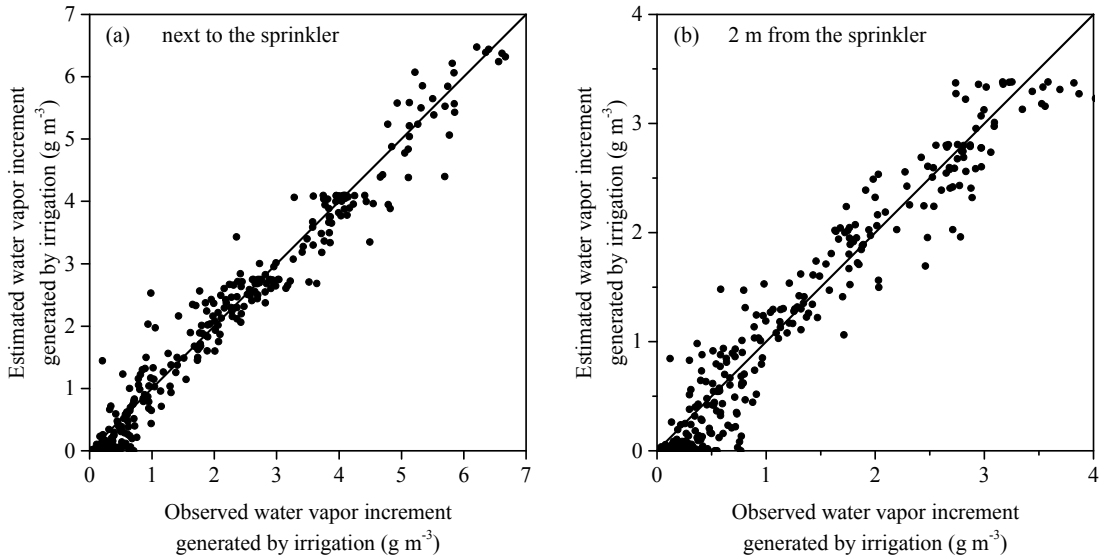

Figure 6. Comparison between observed and estimated water vapor increment due to irrigation for all the available tests: next to the sprinkler (**a**) and 2 m from the sprinkler (**b**) The diagonal line indicates a 1:1 relationship.

Table 3. Evaluation of model performance.

Coefficients	Model Performance	
	Next to the Sprinkler	2 m from Sprinkler
SD	1.72	1.04
RMSE	0.34	0.27
n_i	4.05	2.91
Nash—Sutcliffe model efficiency coefficient	0.961	0.934

Notes: *SD*, standard deviation of observations; *RMSE*, root mean square error; n_i, number of times that the observations variability is greater than the mean error.

The model tended to more reliable for relatively low water vapor increment, i.e., lower than approximately 3 and 2 g m^{-3} for observations next to and 2 m from the sprinkler, respectively. This may be due to a decrease in sensor accuracy when relative humidity is relatively high (i.e., >90%) [66,67], such that we expect more fluctuation and instability in water vapor content measurements at higher levels.

In addition, the estimated values tended to be underestimated when the values of water vapor increment were lower than 0.5 g m^{-3}. This may be because the observed values did not tend toward zero, due to the interference of meteorological fluctuations and evaporation from soil and vegetation, during the period 2–3 h following the completion of irrigation [16,68]. However, during this period, the trend of water vapor increment estimated by the model was reduced and steadily approached zero.

5. Conclusions

The water vapor dynamics during and after irrigation for a single overhead sprinkler are not clear. The current study revealed the dynamic variations of water vapor increment during and after irrigation, and a dynamic model was developed to describe the water vapor dynamics during and

after irrigation. The model can be used to quantitatively describe water vapor increment at any time during and after irrigation. This work should be beneficial for determining the characteristics of WDEL and for proposing relevant strategies or measures to decrease water losses and increase the water use efficiency.

The water vapor dynamics model showed that the fitting was in good agreement between measured values and the developed model for water vapor increment next to and 2 m from the sprinkler. The adjusted coefficients of determination of the fitting were 0.644 to 0.947 and 0.759 to 0.980, for periods during and after irrigation, respectively. The values of the Nash-Sutcliffe efficiency coefficient were 0.961 and 0.934 for estimations next to the sprinkler and for 2 m away from the sprinkler, respectively, suggesting a very good model performance.

During irrigation, the water vapor dynamics increased rapidly, as soon as the irrigation started, and then the rate of increase leveled off until it reached a maximum content, which suggests that dynamics can be expressed by an exponential equation. After irrigation finished, water vapor dynamics gradually moved from a stable state to a decreasing trend, and then rapidly decreased; finally, the decreasing rate leveled off to zero, when the water vapor content was restored to the level of the surrounding atmosphere, which suggests that the dynamics can be expressed by a logistic equation during this period.

As a reference for the model parameter A_s, the maximum amounts of water vapor increment generated by irrigation were 2.506 to 6.476 g m^{-3} and 1.277 to 3.380 g m^{-3} for the areas next to and 2 m from the sprinkler, respectively.

For the irrigation period, the lower the VPD, the lower the maximum water vapor increment in the area 2 m from the sprinkler. However, the VPD had no obvious influence on water vapor increment in the area next to the sprinkler. The meteorological conditions involving temperature, relative humidity, and VPD influenced the increasing and decreasing rates of dynamics of water vapor increment. With different meteorological conditions, a period of 2.3 to 4.0 h was needed for the water vapor to be restored to the atmospheric level.

The developed model can be used to describe water vapor dynamics during and after irrigation, and to estimate the water vapor characteristics, including the maximum content and increasing and decreasing rates of change in water vapor increment, with overhead sprinkler irrigation and low wind conditions.

Acknowledgments: This work was supported by the National Natural Science Foundation of China (No. 51379011). The authors would like to thank the support provided by the staff and technicians associated with the Clover Group Shuangqiao Experimental Base: Yishan Liu, Jianming Sun and Pai Hou. We are grateful to Yandong Zhao and Zhitao Gao for technical support for the water vapor measurement systems. Certain products utilized in this study do not imply any endorsements of them.

Author Contributions: Jian Jiao and Derong Su conceived and designed the experiments; Jian Jiao and Yadong Wang performed the experiments; Jian Jiao analyzed the data and wrote the paper. Both authors read and approved the manuscript.

Conflicts of Interest: The authors declare no conflict of interest. The founding sponsors had no role in the design of the study; in the collection, analyses, or interpretation of data; in the writing of the manuscript, and in the decision to publish the results.

References

1. Boucher, O.; Myhre, G.; Myhre, A. Direct human influence of irrigation on atmospheric water vapour and climate. *Clim. Dyn.* **2004**, *22*, 597–603. [CrossRef]
2. Douglas, E.M.; Niyogi, D.; Frolking, S.; Yeluripati, J.B.; Pielke, R.A.; Niyogi, N.; Vörösmarty, C.J.; Mohanty, U.C. Changes in moisture and energy fluxes due to agricultural land use and irrigation in the Indian Monsoon Belt. *Geophys. Res. Lett.* **2006**, *33*, 70–84. [CrossRef]
3. Jaramillo, F.; Destouni, G. Local flow regulation and irrigation raise global human water consumption and footprint. *Science* **2015**, *350*, 1248–1251. [CrossRef] [PubMed]

4. Rost, S.; Gerten, D.; Bondeau, A.; Lucht, W.; Rohwer, J.; Schaphoff, S. Agricultural green and blue water consumption and its influence on the global water system. *Water Resour. Res.* **2008**, *44*, 137–148. [CrossRef]
5. Wada, Y.; Van Beek, L.P.; Wanders, N.; Bierkens, M.F. Human water consumption intensifies hydrological drought worldwide. *Environ. Res. Lett.* **2013**, *8*, 034036. [CrossRef]
6. Sun, Q.Z.; Yu, Z.; Ma, C.H.; Xu, C.C. Achievements of the alfalfa industry in last decade and priorities in next decade in China. *Pratacult. Sci.* **2013**, *30*, 471–477.
7. Li, L.; Li, N.; Sheng, J.D.; Wang, H. Effects of nitrogen fertilizer and planting density on alfalfa growth and seed yield. *Acta Agrestia Sin.* **2012**, *20*, 54–57.
8. Urrego-Pereira, Y.; Cavero, J.; Medina, E.; Martínez-Cob, A. Role of transpiration reduction during center-pivot sprinkler irrigation in application efficiency. *J. Irrig. Drain. Eng.* **2013**, *139*, 221–232. [CrossRef]
9. Ouazaa, S.; Latorre, B.; Burguete, J.; Serreta, A.; Playán, E.; Salvador, R.; Paniagua, P.; Zapata, N. Effect of the start-stop cycle of center-pivot towers on irrigation performance: Experiments and simulations. *Agric. Water Manag.* **2015**, *147*, 163–174. [CrossRef]
10. Foley, J.P. Centre pivot and lateral move machines. In *WATERpak A Guide for Irrigation Management in Cotton*; Cotton Research and Development Corporation: Narrabri, Australia, 2008; pp. 195–220.
11. Chalfant, R.B.; Young, J.R. Chemigation, or application of insecticide through overhead sprinkler irrigation systems, to manage insect pests infesting vegetable and agronomic crops. *J. Econ. Entomol.* **1982**, *75*, 237–241. [CrossRef]
12. Omary, M.; Camp, C.R.; Sadler, E.J. Center pivot irrigation system modification to provide variable water application depths. *Trans. ASAE* **1997**, *13*, 235–239.
13. Faci, J.; Salvador, R.; Playán, E.; Sourell, H. Comparison of fixed and rotating spray plate sprinklers. *J. Irrig. Drain. Eng.* **2001**, *127*, 224–233. [CrossRef]
14. Smajstrla, A.G.; Zazueta, F. *Evaporation Loss during Sprinkler Irrigation*; University of Florida Cooperative Extension Service, Institute of Food and Agriculture Sciences; EDIS: Gainesville, FL, USA, 1994.
15. Uddin, J.; Smith, R.; Hancock, N.; Foley, J.P. Droplet evaporation losses during sprinkler irrigation: An overview. In *Proceedings of the Australian Irrigation Conference and Exibition, Sydney, Australia*; Irrigation Australia Ltd.: Sydney, Australia, 2010; pp. 1–10.
16. Stambouli, T.; Martinez-Cob, A.; Faci, J.M.; Howell, T.; Zapata, N. Sprinkler evaporation losses in alfalfa during solid-set sprinkler irrigation in semiarid areas. *Irrig. Sci.* **2013**, *31*, 1075–1089. [CrossRef]
17. Kohl, R.; Wright, J. Air temperature and vapor pressure changes caused by sprinkler irrigation. *Agron. J.* **1974**, *66*, 85–88. [CrossRef]
18. Steiner, J.L.; Kanemasu, E.T.; Clark, R.N. Spray losses and partitioning of water under a center pivot sprinkler system. *Trans. ASAE* **1983**, *26*, 1128–1134. [CrossRef]
19. ASAE Standards. *Test Procedure for Determining the Uniformity of Water Distribution of Centre Pivot, Corner Pivot and Moving Lateral Irrigation Machines Equipped with Spray or Sprinkler Nozzles*; ASAE: St. Joseph, MI, USA, 1995; Volume ANSI/ASAE S436.1.
20. ISO 11545:2009. *Agricultural Irrigation Equipment—Centre-Pivot and Moving Lateral Irrigation Machines with Sprayer or Sprinkler Nozzles—Determination of Uniformity of Water Distribution*; ISO: Geneva, Switzerland, 2009; Volume ISO-11545.
21. Tarjuelo, J.M.; Ortega, J.F.; Montero, J.; de Juan, J.A. Modelling evaporation and drift losses in irrigation with medium size impact sprinklers under semi-arid conditions. *Agric. Water Manag.* **2000**, *43*, 263–284. [CrossRef]
22. Dechmi, F.; Playán, E.; Cavero, J.; Faci, J.; Martínez-Cob, A. Wind effects on solid set sprinkler irrigation depth and yield of maize (Zea mays). *Irrig. Sci.* **2003**, *22*, 67–77. [CrossRef]
23. Playán, E.; Salvador, R.; Faci, J.M.; Zapata, N.; Martínez-Cob, A.; Sánchez, I. Day and night wind drift and evaporation losses in sprinkler solid-sets and moving laterals. *Agric. Water Manag.* **2005**, *76*, 139–159. [CrossRef]
24. Ortíz, J.N.; Tarjuelo, J.M.; de Juan, J.A. Characterisation of evaporation and drift losses with centre pivots. *Agric. Water Manag.* **2009**, *96*, 1541–1546. [CrossRef]
25. Sanchez, I.; Zapata, N.; Faci, J.M. Combined effect of technical, meteorological and agronomical factors on solid-set sprinkler irrigation: II. Modifications of the wind velocity and of the water interception plane by the crop canopy. *Agric. Water Manag.* **2010**, *97*, 1591–1601. [CrossRef]

26. Martínez-Cob, A.; Playán, E.; Zapata, N.; Cavero, J.; Medina, E.; Puig, M. Contribution of evapotranspiration reduction during sprinkler irrigation to application efficiency. *J. Irrig. Drain. Eng.* **2008**, *134*, 745–756. [CrossRef]
27. Sanchez, I.; Faci, J.M.; Zapata, N. The effects of pressure, nozzle diameter and meteorological conditions on the performance of agricultural impact sprinklers. *Agric. Water Manag.* **2011**, *102*, 13–24. [CrossRef]
28. Playán, E.; Garrido, S.; Faci, J.M.; Galán, A. Characterizing pivot sprinklers using an experimental irrigation machine. *Agric. Water Manag.* **2004**, *70*, 177–193. [CrossRef]
29. Sadeghi, S.-H.; Peters, T.R.; Amini, M.Z.; Malone, S.L.; Loescher, H.W. Novel approach to evaluate the dynamic variation of wind drift and evaporation losses under moving irrigation systems. *Biosyst. Eng.* **2015**, *135*, 44–53. [CrossRef]
30. George, T.J. Evaporation from Irrigation Sprinkler Sprays as Determined by an Electrical Conductivity Method. Master's Thesis, University of California, Davis, CA, USA, 1955.
31. Kohl, K.D.; Kohl, R.A.; Deboer, D.W. Measurement of low pressure sprinkler evaporation loss. *Trans. ASAE* **1987**, *30*, 1071–1074. [CrossRef]
32. Uddin, J.; Smith, R.J.; Hancock, N.H.; Foley, J.P. Evaporation and sapflow dynamics during sprinkler irrigation of cotton. *Agric. Water Manag.* **2013**, *125*, 35–45. [CrossRef]
33. Faci, J.; Bercero, A. Wind effect on irrigation uniformity and on evaporation and wind drift losses in sprinkler systems. *Investig. Agrar. Prod. Prot. Veg.* **1991**, *6*, 171–182.
34. Colombo, A.; Faria, L.C.; Silva, J.J.D.S.J.; Sant Ana, J.A.D.V.S.A.; Beskow, S.; Nörenberg, B.G.N. Modeling of evaporation and wind drift losses in rotating spray plate sprinklers. *Rev. Bras. Eng. Agric. Ambient* **2015**, *19*, 719–726. [CrossRef]
35. Dechmi, F.; Playan, E.; Faci, J.; Tejero, M.; Bercero, A. Analysis of an irrigation district in northeastern spain: II. Irrigation evaluation, simulation and scheduling. *Agric. Water Manag.* **2003**, *61*, 93–109. [CrossRef]
36. Beskow, S.; Faria, L.C.; Colombo, A.; Moura, D.C.M. Modeling of evaporation and wind drift losses in medium-pressure sprinklers. *Rev. Bras. Eng. Agric. Ambient.* **2011**, *15*, 221–228. [CrossRef]
37. Yan, H.J.; Bai, G.; He, J.Q.; Li, Y.J. Model of droplet dynamics and evaporation for sprinkler irrigation. *Biosyst. Eng.* **2010**, *106*, 440–447. [CrossRef]
38. De Wrachien, D.; Lorenzini, G. Modelling jet flow and losses in sprinkler irrigation: Overview and perspective of a new approach. *Biosyst. Eng.* **2006**, *94*, 297–309. [CrossRef]
39. Liu, H.J.; Kang, Y.H. Effect of sprinkler irrigation on microclimate in the winter wheat field in the North China Plain. *Agric. Water Manag.* **2006**, *84*, 3–19. [CrossRef]
40. Wang, D.; Li, J.; Rao, M. Estimation of net interception loss by crop canopy under sprinkler irrigation based on energy balance. *Trans. Chin. Soc. Agric. Eng.* **2007**, *23*, 27–33.
41. Vaisala, O. *Humidity Conversion Formulas*; Vaisala Oyj: Helsinki, Finland, 2012.
42. Allen, R.G.; Pereira, L.S.; Raes, D.; Smith, M. *Crop Evapotranspiration-Guidelines for Computing Crop Water Requirements*; FAO Irrigation and Drainage Paper 56; FAO: Rome, Italy, 1998.
43. Tsoularis, A.; Wallace, J. Analysis of logistic growth models. *Math. Biosci.* **2002**, *179*, 21–55. [CrossRef]
44. Verhulst, P.F. Notice sur la loi que la population suit dans son accroissement. *Corresp. Math. Phys.* **1838**, *10*, 113–121.
45. Andrewartha, H.G.; Birch, L.C. *The Distribution and Abundance of Animals*; University of Chicago Press: Chicago, IL, USA, 1954.
46. Cavero, J.; Jiménez, L.; Puig, M.; Faci, J.M.; Martínez-Cob, A. Maize growth and yield under daytime and nighttime solid-set sprinkler irrigation. *Agron. J.* **2008**, *100*, 1573–1579. [CrossRef]
47. Nash, J.E.; Sutcliffe, J.V. River flow forecasting through conceptual models part I—A discussion of principles. *J. Hydrol.* **1970**, *10*, 282–290. [CrossRef]
48. Ritter, A.; Muñoz-Carpena, R. Performance evaluation of hydrological models: Statistical significance for reducing subjectivity in goodness-of-fit assessments. *J. Hydrol.* **2013**, *480*, 33–45. [CrossRef]
49. *OriginPro Originlab Originpro Version 9.2*; OriginPro Corp.: Northampton, MA, USA, 2014.
50. Argus. Understanding and Using vpd. Argus Application Note. Available online: http://www.arguscontrols.com/resources/VPD_Application_Note.pdf (accessed on 9 November 2016).
51. Leonardi, C.; Guichard, S.; Bertin, N. High vapour pressure deficit influences growth, transpiration and quality of tomato fruits. *Sci. Hortic.* **2000**, *84*, 285–296. [CrossRef]

52. Urrego-Pereira, Y.; Cavero, J.; Medina, E.T.; Martínez-Cob, A. Microclimatic and physiological changes under a center pivot system irrigating maize. *Agric. Water Manag.* **2013**, *119*, 19–31. [CrossRef]
53. Sayyadi, H.; Nazemi, A.H.; Sadraddini, A.A.; Delirhasannia, R. Characterising droplets and precipitation profiles of a fixed spray-plate sprinkler. *Biosyst. Eng.* **2014**, *119*, 13–24. [CrossRef]
54. Raviv, M. *Soilless Culture: Theory and Practice*; Elsevier: Amsterdam, The Netherlands, 2007.
55. Stambouli, T.; Zapata, N.; Faci, J.M. Performance of new agricultural impact sprinkler fitted with plastic nozzles. *Biosyst. Eng.* **2014**, *118*, 39–51. [CrossRef]
56. Yazar, A. Evaporation and drift losses from sprinkler irrigation systems under various operating conditions. *Agric. Water Manag.* **1984**, *8*, 439–449. [CrossRef]
57. Cavero, J.; Medina, E.; Puig, M.; Martínez-Cob, A. Sprinkler irrigation changes maize canopy microclimate and crop water status, transpiration, and temperature. *Agron. J.* **2009**, *101*, 854–864. [CrossRef]
58. Zhao, W.X.; Li, J.S.; Li, Y.F. Modeling sprinkler efficiency with consideration of microclimate modification effects. *Agric. For. Meteorol.* **2012**, *161*, 116–122. [CrossRef]
59. Weaver, H.L. Temperature and humidity flux-variance relations determined by one-dimensional eddy correlation. *Bound. Lay. Meteorol.* **1990**, *53*, 77–91. [CrossRef]
60. Kinoshita, N. Nonuniform distribution of high-frequency turbulence in the unstable boundary layer. *Bound. Lay. Meteorol.* **2003**, *106*, 61–91. [CrossRef]
61. Krause, P.; Boyle, D.; Bäse, F. Comparison of different efficiency criteria for hydrological model assessment. *Adv. Geosci.* **2005**, *5*, 89–97. [CrossRef]
62. Gupta, H.V.; Kling, H.; Yilmaz, K.K.; Martinez, G.F. Decomposition of the mean squared error and nse performance criteria: Implications for improving hydrological modelling. *J. Hydrol.* **2009**, *377*, 80–91. [CrossRef]
63. Suleiman, A.A.; Tojo Soler, C.M.; Hoogenboom, G. Evaluation of FAO-56 crop coefficient procedures for deficit irrigation management of cotton in a humid climate. *Agric. Water Manag.* **2007**, *91*, 33–42. [CrossRef]
64. Fan, J.; Oestergaard, K.T.; Guyot, A.; Lockington, D.A. Measuring and modeling rainfall interception losses by a native banksia woodland and an exotic pine plantation in subtropical coastal Australia. *J. Hydrol.* **2014**, *515*, 156–165. [CrossRef]
65. Fang, Q.; Ma, L.; Yu, Q.; Ahuja, L.R.; Malone, R.W.; Hoogenboom, G. Irrigation strategies to improve the water use efficiency of wheat–maize double cropping systems in north china plain. *Agric. Water Manag.* **2010**, *97*, 1165–1174. [CrossRef]
66. Joshi, S.N.; Pate, M.B.; Nelson, R.M.; House, J.M.; Klaassen, C.J. An experimental evaluation of duct-mounted relative humidity sensors: Part 2-accuracy results. *ASHRAE Trans.* **2005**, *111*, 167–176.
67. Sensirion, A.G. Data Sheet SHT7x (SHT 71, SHT 75)-Humidity and Temperature Sensor IC. Available online: https://www.sensirion.com/fileadmin/user_upload/customers/sensirion/Dokumente/2_Humidity_Sensors/Sensirion_Humidity_Sensors_SHT7x_Datasheet_V5.pdf (accessed on 30 December 2014).
68. Urrego-Pereira, Y.F.; Martínez-Cob, A.; Fernández, V.; Cavero, J. Daytime sprinkler irrigation effects on net photosynthesis of maize and alfalfa. *Agron. J.* **2013**, *105*, 1515–1528. [CrossRef]